nature physics

ARTICLES

PUBLISHED ONLINE: 12 AUGUST 2012 | DOI: 10.1038/NPHYS2380

Decrease of upper critical field with underdoping in cuprate superconductors

J. Chang[1†], N. Doiron-Leyraud[1], O. Cyr-Choinière[1], G. Grissonnanche[1], F. Laliberté[1], E. Hassinger[1], J-Ph. Reid[1], R. Daou[1†], S. Pyon[2], T. Takayama[2], H. Takagi[2,3] and Louis Taillefer[1,4]*

It is still unclear why the transition temperature T_c of cuprate superconductors falls with underdoping. The doping dependence of the critical magnetic field H_{c2} is directly relevant to this question, but different estimates of H_{c2} are in sharp contradiction. We resolve this contradiction by tracking the characteristic field scale of superconducting fluctuations as a function of doping, via measurements of the Nernst effect in $La_{1.8-x}Eu_{0.2}Sr_xCuO_4$. H_{c2} is found to fall with underdoping, with a minimum where stripe order is strong. The same non-monotonic behaviour is observed in the archetypal cuprate superconductor $YBa_2Cu_3O_y$. We conclude that competing states such as stripe order weaken superconductivity and cause both H_{c2} and T_c to fall as cuprates become underdoped.

Two paradigms have been proposed to account for the dome-like region of superconductivity in the temperature-doping phase diagram of cuprate superconductors[1]. In the first, the amplitude of the superconducting order parameter grows monotonically as the doping p is reduced, but its phase is increasingly disordered[2], causing T_c to fall at low p. The signature of this scenario is strong phase fluctuations and a superconducting gap above T_c in the underdoped regime. In the second paradigm, the fall of T_c at low p is due to the onset of a state that competes with superconductivity. The signature of this scenario is a small superconducting gap and a small H_{c2} in the underdoped regime.

Whether strong phase fluctuations or a decrease in the pairing gap is causing T_c to fall in underdoped cuprates is currently an open question. Different interpretations of photoemission data disagree on the evolution of the pairing gap[3–6] and different estimates of the upper critical field H_{c2} are in sharp contradiction[7,8]. The Nernst signal observed above T_c in underdoped cuprates has been attributed to superconducting fluctuations[8–10], and because it persists up to temperatures several times T_c, it was deemed incompatible with the standard Gaussian fluctuations of the superconducting order parameter. It was attributed instead to vortex-like excitations in a phase-fluctuating superconductor[9,10] with a non-zero pairing amplitude above T_c. The critical field H_{c2} deduced from the Nernst data on cuprates such as $Bi_2Sr_2CaCu_2O_{8+\delta}$ (Bi-2212) was reported to increase with underdoping[8], even though T_c falls. As shown in Fig. 1a, this is in striking contrast to the rapid drop in H_{c2} deduced from a Gaussian analysis of fluctuations in the magneto-conductivity of $YBa_2Cu_3O_y$ (YBCO; ref. 7).

Nernst effect in Eu–LSCO

Here we re-examine the Nernst effect in cuprates with a study of $La_{1.8-x}Eu_{0.2}Sr_xCuO_4$ (Eu–LSCO), an underdoped cuprate in which the ratio of superconducting (N_{sc}) to quasiparticle (N_{qp}) contributions to the Nernst signal N is exceptionally large—at least 100 times larger than in previous studies of superconducting fluctuations in cuprates (see Supplementary Table S2). Because of its low T_c, we could determine the quasiparticle background $N_{qp}(T)$ in Eu–LSCO by fully suppressing superconductivity with a magnetic field (Fig. 2a). The large signal-to-background ratio allows us to reliably track N_{sc} up to high temperature, namely up to a reduced temperature $\varepsilon \equiv (T-T_c)/T_c \approx 5$, compared to a typical upper limit of $\varepsilon \approx 0.5$. As we shall see, this gives us access to a regime where the complicating effects of paraconductivity are negligible.

In Fig. 3a, N_{sc} is plotted versus magnetic field H for different temperatures above T_c, for Eu–LSCO at a doping $p = 0.11$. N_{sc} increases linearly at low H, peaks at a field H^* and then decreases monotonically at high H, just as in the conventional superconductor $Nb_{0.15}Si_{0.85}$ (refs 11,12; Supplementary Fig. S2). The peak field H^*, also called the 'ghost critical field' (ref. 12), is plotted versus ε in Fig. 3b. It obeys $H^* = H^*_{c2}\ln(T/T_c)$ from $\varepsilon \approx 0.5$ to $\varepsilon \approx 5$, where H^*_{c2} is a field scale whose relation to the $T = 0$ upper critical field H_{c2} is discussed below.

Below $\varepsilon \approx 0.5$, H^* deviates from $\ln(T/T_c)$, and remains finite as $\varepsilon \to 0$. This is because $N_{sc}(\varepsilon) = \alpha^{sc}_{xy}(\varepsilon)/\sigma(\varepsilon)$ is the ratio of two quantities[13–16]—the off-diagonal Peltier coefficient from superconducting fluctuations α^{sc}_{xy} and the electrical conductivity σ—which both diverge as $\varepsilon \to 0$ (ref. 13). This causes N_{sc} to saturate at low ε (Fig. 4). The deviation of H^* from $\ln(T/T_c)$ coincides with the onset of paraconductivity below $T \approx 6\,\mathrm{K} \approx 1.5T_c$ (see Supplementary Fig. S3 and Fig. 4c inset). Above $\varepsilon \approx 0.5$, paraconductivity is negligible (Supplementary Fig. S4) and σ reaches its (field-independent) normal-state value, at which point $N_{sc}(H) \sim \alpha^{sc}_{xy}(H)$. We make use of H^* in the latter regime only.

H^* also obeys $H^* = H^*_{c2}\ln(T/T_c)$ in our other Eu–LSCO samples (Supplementary Table S1 and Fig. S1), with $p = 0.08$, 0.10 and 0.125 (Fig. 3c). The value of H^*_{c2} extracted from the fit at each doping is plotted in Fig. 5a. Our first and main finding is this: the field scale for superconductivity, H^*_{c2}, decreases with underdoping, in a non-monotonic way, with a local minimum at $p = 0.11$. This

[1]Département de physique and RQMP, Université de Sherbrooke, Sherbrooke, Québec J1K 2R1, Canada, [2]Department of Advanced Materials, University of Tokyo, Kashiwa 277-8561, Japan, [3]RIKEN (The Institute of Physical and Chemical Research), Wako 351-0198, Japan, [4]Canadian Institute for Advanced Research, Toronto, Ontario M5G 1Z8, Canada. †Present addresses: Institut de Physique de la Matière Complexe, École Polytechnique Fédérale de Lausanne (EPFL), CH-1015 Lausanne, Switzerland & Paul Scherrer Institut, CH-5232 Villigen, Switzerland (J.C.); Laboratoire de Cristallographie et Sciences des Matériaux, CNRS (UMR6508), Caen 14050, France (R.D.). *e-mail: louis.taillefer@usherbrooke.ca.

© 2012 Macmillan Publishers Limited. All rights reserved.

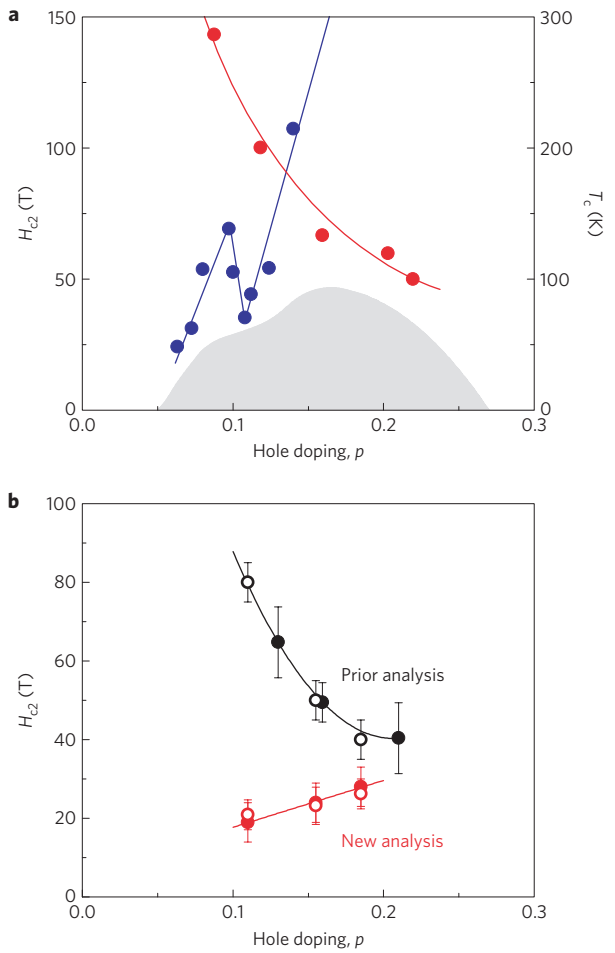

Figure 1 | Doping dependence of the upper critical field H_{c2} in cuprate superconductors. a, Upper critical field H_{c2} of cuprate superconductors versus doping p extracted from magneto-conductivity data on YBCO (ref. 7, blue circles; left axis) and from Nernst data on Bi-2212 (ref. 8, red circles; left axis). These two studies of superconducting fluctuations above T_c led to contradictory conclusions on how the superconducting pairing strength in cuprates varies with doping. The superconducting T_c of YBCO is also shown (ref. 34, grey dome; right axis). **b**, Two different definitions of the upper critical field H_{c2} extracted from Nernst data on the same material, Bi-2201, lead to opposite doping dependencies. When H_{c2} is defined as the field H where N versus H at $T = T_c$ extrapolates to zero (filled black circles and error bars, from ref. 8), one finds that H_{c2} increases with underdoping. The same increase is found for the peak field H^* in N versus H (see Fig. 3a) when taken at $T = T_c$ (open black circles; from Fig. 7, ×10). By contrast, a decrease is found if the peak field H^* is taken at $T \approx 1.65T_c$ ($\varepsilon \approx 0.65$), outside the region of strong paraconductivity (open red circles; from Fig. 7, ×1.9). The latter result is independent of any theory. Equivalently, H_{c2} may be obtained as H^*_{c2} in a fit of the peak field H^* to $H^*_{c2}\ln(T/T_c)$ (see Fig. 3b), as done in Fig. 7 (filled red circles), again yielding an H_{c2} that decreases with underdoping. This is true whether H^* is obtained from Nernst data (away from the region of strong paraconductivity) or from diamagnetism (Fig. 7). The error bars on the filled red circles reflect the uncertainty in fitting the H^* data points in Fig. 7 to the relation $H^*_{c2}\ln(T/T_c)$. Error bars on open circles (red and black) reflect the uncertainty in determining H^* from the data in refs 10,20 (see Fig. 7).

result comes directly from the Nernst data, free of any model or theory. In fact, the evolution of H^*_{c2} may be directly read off the raw N versus H isotherms: it is simply proportional to the field H^* at which N peaks for a given reduced temperature, say $T = 1.5T_c$ (Supplementary Fig. S5).

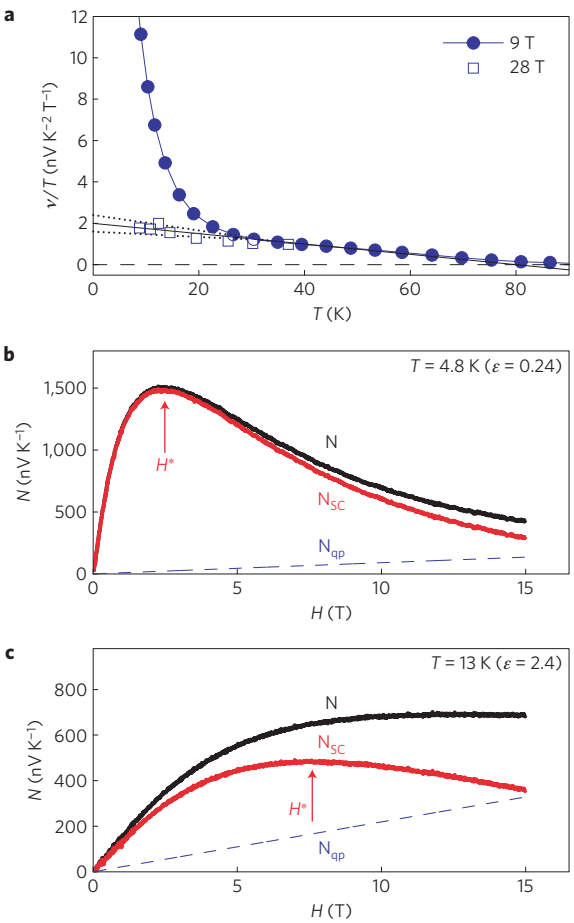

Figure 2 | Quasiparticle and superconducting contributions to the Nernst signal in Eu-LSCO. a, Temperature dependence of the Nernst coefficient $\nu \equiv N/H$ of Eu-LSCO at $p = 0.125$, plotted as ν/T versus T, for two magnetic fields as indicated. $\nu(T)$ is independent of H for $T > 35$ K, and hence $\nu(T) \approx \nu_{qp}(T)$ above 35 K (ref. 32). In the range 35–70 K, ν/T is linear, so that $\nu_{qp}/T = a - bT$ (solid black line). Application of a field of 28 T (open squares) to suppress superconductivity such that $\nu_{sc} \ll \nu_{qp}$ shows that the linear T dependence of $\nu_{qp}(T)$ persists as $T \to 0$. We therefore take $N_{qp} = \nu_{qp}H = (a - bT)TH$ to be our estimate of the quasiparticle contribution used to extract $N_{sc}(T,H) = N(T,H) - N_{qp}(T)$. The same procedure is applied to the data at $p = 0.08$, 0.10 and 0.11, with parameters a and b that are only slightly different. The dashed lines are the upper and lower bounds on the uncertainty in $\nu_{qp}(T)$. These translate into error bars in the determination of H^* plotted in Fig. 3b,c (see panels below). **b**,**c**, Nernst signal $N = \nu H$ (black) measured in Eu-LSCO at $p = 0.11$ and quasiparticle contribution $N_{qp} = \nu_{qp}H$ (dashed blue line), for two temperatures as indicated. The difference $N_{sc} = N - N_{qp}$ (red) is the contribution of superconducting fluctuations. In **b**, where $\varepsilon < 1$, N_{qp} is small compared with the measured Nernst signal and hence the extraction of the peak field H^*, defined as the field where N_{sc} versus H is maximal, is essentially unaffected by the subtraction of N_{qp}. By contrast for $\varepsilon > 1$ (**c**), N_{qp} is large and subtraction is necessary to obtain an accurate determination of H^*.

Nernst data on $Nb_{0.15}Si_{0.85}$ (refs 11,12) yield a peak field in agreement with $H^* = H^*_{c2}\ln(T/T_c)$ up to at least 5 T_c (Fig. 3c). Pourret *et al.* point out that H^* separates a low-H regime controlled by the temperature-dependent coherence length $\xi(T) = \xi_0/(\ln(T/T_c))^{1/2}$ and a high-H regime controlled by the magnetic length $l_B = (h/2eH)^{1/2}$ (ref. 17) where ξ_0 is the $T = 0$ superconducting coherence length, h is Planck's constant, and e is the electron charge. They argue that H^* is the field where $\xi(T) = l_B(H^*)$, so that $H^* = (\Phi_0/2\pi\xi_0^2)\ln(T/T_c)$, where $\Phi_0 = h/2e$ is the flux quantum.

© 2012 Macmillan Publishers Limited. All rights reserved.

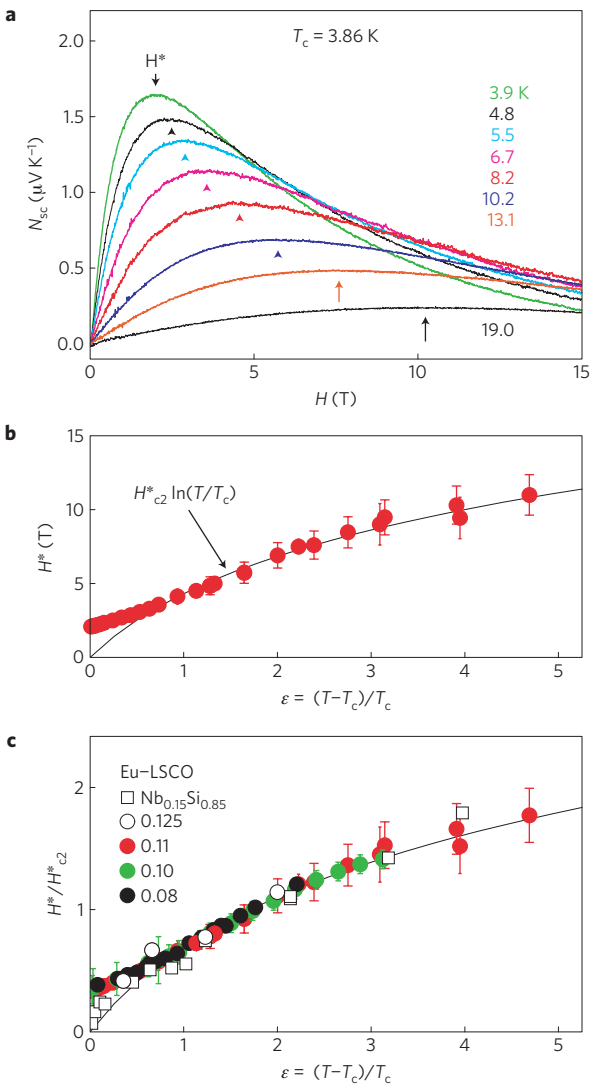

Figure 3 | Peak field H^* in the superconducting Nernst signal above T_c. **a**, Superconducting Nernst signal N_{sc} of Eu-LSCO plotted as a function of magnetic field H at $p = 0.11$, for different values of the temperature T as indicated. A quasiparticle background N_{qp} is subtracted from the raw data of N versus H in Supplementary Fig. S1 (see Fig. 2). The arrows mark the maximum value of $N_{sc} = N - N_{qp}$ for each isotherm, which defines the peak field H^* (also called the 'ghost critical field'). **b**, Temperature dependence of H^* extracted from the data in **a** plotted versus reduced temperature $\varepsilon \equiv (T - T_c)/T_c$. The solid line is a fit to $H^* = H^*_{c2} \ln(T/T_c)$, which provides a model-free field scale, H^*_{c2}, equal to 6.2 T for this doping. **c**, Peak field H^* in Eu-LSCO at $p = 0.08$, 0.10, 0.11 and 0.125, and in the conventional superconductor $Nb_{0.15}Si_{0.85}$ (from ref. 11), plotted as H^*/H^*_{c2} versus ε, with H^*_{c2} obtained as in **b** for each sample. The values of H^*_{c2} are given in Supplementary Table S1 and plotted in Fig. 5a. Error bars on H^* in **b** and **c** come from the uncertainty in N_{qp} (Fig. 2).

This makes the field scale H^*_{c2} equal to the $T = 0$ upper critical field $H_{c2} \equiv \Phi_0/2\pi\xi_0^2$. In Supplementary Fig. S6, we use resistivity data on Nd–LSCO, a material very similar to Eu–LSCO, to show that the field H^{res}_{c2} needed to suppress superconductivity in Nd–LSCO at $p = 0.12$ and $T = T_c/20$ is roughly equal to H^*_{c2} in Eu–LSCO at $p = 0.125$ (Fig. 5a). This confirms experimentally that $H^*_{c2} \approx H_{c2}$.

Comparison to Gaussian theory

We now compare our data against the theory of Gaussian fluctuations[13–15]. The calculated curve of α^{sc}_{xy} versus H (ref. 15) is in excellent agreement with the measured curve of N_{sc} versus H (Fig. 6). The peak field in α^{sc}_{xy} versus H increases with temperature roughly as $H^* \sim \ln(T/T_c)$ (Supplementary Fig. S7), with a prefactor that is proportional to $1/\xi_0^2$ (Supplementary Fig. S7). In the $H = 0$ limit, theory predicts[14,15]: $\nu_{sc}\,\sigma = \alpha^{sc}_{xy}/H \sim \xi_0^2/T\ln(T/T_c)$. In Fig. 4a, the Nernst coefficient $\nu(\equiv N/H)$ of Eu–LSCO at $p = 0.11$ is plotted versus H for different temperatures above T_c. Its value in the $H = 0$ limit, $\nu_0 \equiv \nu(H \to 0)$, is plotted in Fig. 4b as a function of ε. In Fig. 4d, the data are seen to follow the theoretical temperature dependence precisely, from 1.02 T_c up to at least 5 T_c, as previously found[14,15] in $Nb_{0.15}Si_{0.85}$ (refs 11,12). As shown in Fig. 6 (and explained in the Supplementary Information), the data also follow the theoretical dependence on magnetic field, both at $T < T_c$ and at $T > T_c$. We conclude that our Nernst data on Eu–LSCO are consistent with several non-trivial features of Gaussian theory. This validates the earlier use of Gaussian theory to analyse conductivity data[7] in YBCO (in a context of much smaller signal-to-background ratio; Supplementary Table S2), discussed below. Note that the quantum oscillations observed in YBCO at $p \sim 0.1$ (ref. 18) are consistent with Fermi-liquid theory[19], the framework on which Gaussian theory is based. Agreement with Gaussian theory and consistency of the different measures of H_{c2} indicate that the superconducting fluctuations in this cuprate are controlled entirely by the coherence length, and there is only one temperature scale, T_c, and one field scale, H_{c2}, for superconductivity. The fluctuations seem to be no different from those of conventional superconductors, and there is no need to invoke unusual vortex-like excitations[8–10,16,20,21], at least for $p = 0.08$ and above.

Nernst effect and diamagnetism in Bi-2201

Wang *et al.*[8] extracted a field scale from their raw Nernst data on the cuprates Bi-2212 and $Bi_2Sr_{2-y}La_yCu_2O_6$ (Bi-2201), and found it to increase with underdoping (Fig. 1). However, because they used Nernst data at $T = T_c$, their analysis was contaminated by paraconductivity. Our analysis of their data[8] away from T_c yields a field scale that decreases with underdoping, in agreement with diamagnetism data[20] on Bi-2201 (Fig. 7). The H dependence of M_d, the diamagnetic component of magnetization, is very similar to that of N_{sc} (ref. 21), as expected theoretically[16,22]. Magnetization data on an underdoped sample of Bi-2201 with $T_c = 12$ K (ref. 20) yield a peak value H^*_d that obeys $H^*_{c2}\ln(T/T_c)$ all the way from $T \approx T_c$ to $T \approx 4T_c$ (Fig. 7), with $H^*_{c2} \approx 19$ T. Applying the same fit to published Nernst data on a Bi-2201 sample of the same doping[8] yields the same value of H^*_{c2} (Figs 1b and 7). In summary, both diamagnetic and Nernst signals in the cuprate Bi-2201 obey the relation $H^* = H^*_{c2}\ln(T/T_c)$ (Fig. 7), from which the same field scale can be reliably extracted, and this field scale (proportional to H_{c2}) decreases with underdoping (Fig. 1b). This resolves the apparent contradiction highlighted in Fig. 1a.

Critical field H_{c2} in YBCO

In YBCO, a cuprate with $T_c \approx 60$ K at $p = 0.11$, the effect of superconducting fluctuations on the in-plane electrical conductivity σ was analysed up to $\varepsilon \approx 1$ for a range of dopings[7], using the Aslamazov–Larkin theory of Gaussian fluctuations. The only fit parameter in the theory is ξ_0, plotted in Fig. 5a as $H_{c2} = \Phi_0/2\pi\xi_0^2$ versus p. H_{c2} is seen to have a minimum at $p = 0.11$, just as in Eu–LSCO. In Fig. 5b, we show that this value of H_{c2} (obtained from fluctuations above T_c) is in good agreement with the value of H^{res}_{c2} measured at $T \ll T_c$ directly by high-field transport[23,24]. H^{res}_{c2} is defined as the field where ρ or the Hall coefficient R_H or the Seebeck coefficient S has reached its normal-state value[23,24]. For example, in YBCO at $p = 0.11$, S versus H at $T = 2$ K yields $H^{res}_{c2} \approx 25$ T (ref. 24). A third, independent estimate of the coherence length ξ_0 is the vortex core radius measured by muon spin relaxation deep in the vortex state (at low H and $T \ll T_c$). In YBCO at

© 2012 Macmillan Publishers Limited. All rights reserved.

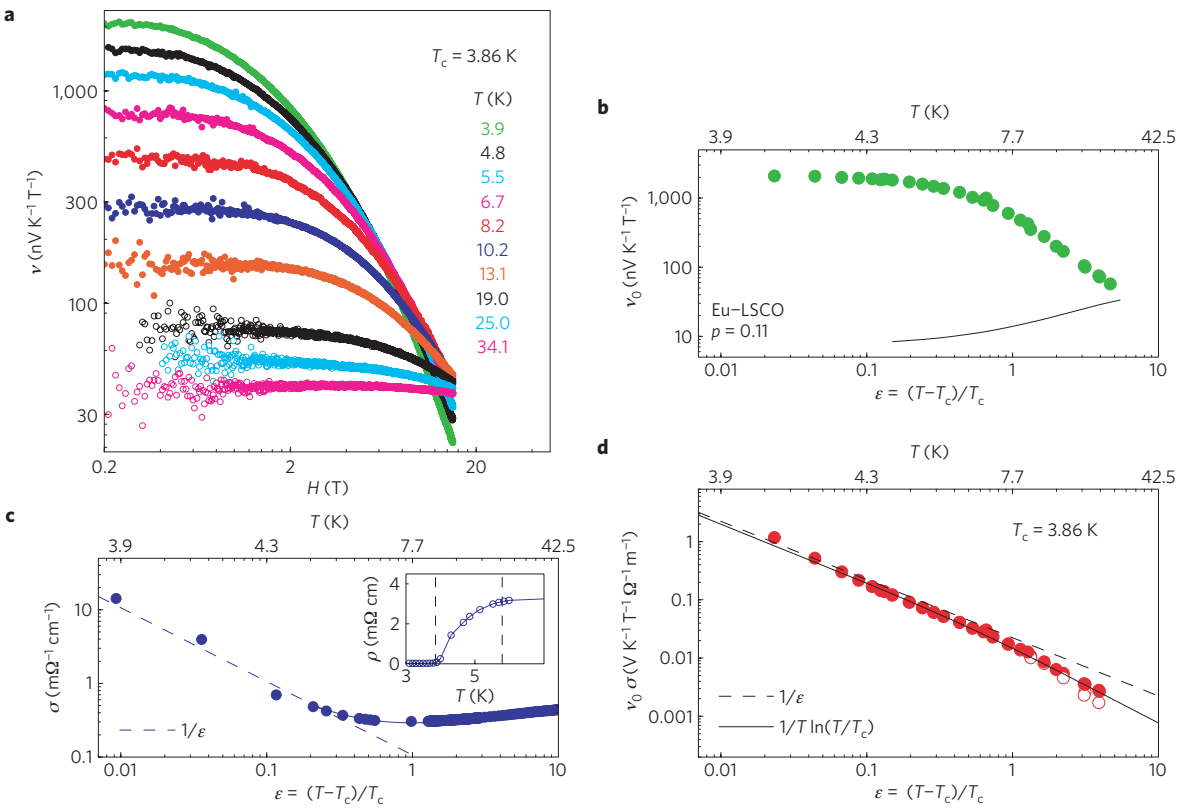

Figure 4 | Temperature dependence: comparison to Gaussian theory. a, Nernst coefficient ν of Eu-LSCO at $p = 0.11$ as a function of magnetic field H, plotted on a log–log scale for various values of the temperature T as indicated. **b**, Temperature dependence of the Nernst coefficient in the $H = 0$ limit, ν_0, plotted versus reduced temperature ε on a log–log scale. The solid line is the quasiparticle background ν_{qp} obtained in Fig. 2. **c**, Zero-field conductivity $\sigma(=1/\rho)$ from Supplementary Fig. S3. The dashed line shows the temperature dependence expected from Gaussian fluctuation theory close to T_c (ref. 13). Inset: zoom on the resistivity near the transition. The lower vertical dashed line marks $T_c = 3.86$ K; the upper vertical dashed line marks $T = 1.5T_c$. **d**, Product of ν_0 in **b** and σ in **c**. Open circles show the effect of subtracting ν_{qp} from ν_0, to obtain $\nu_{sc}(B \to 0) = \nu_0 - \nu_{qp}$. The solid line is the theoretical expectation for the Peltier coefficient in the $B \to 0$ limit, $\alpha_{xy}^{sc} \sim \nu_{sc}\sigma$, from Gaussian fluctuations of the order parameter in a 2D superconductor[14,15]. The dashed line is the expected limiting behaviour close to T_c (ref. 13).

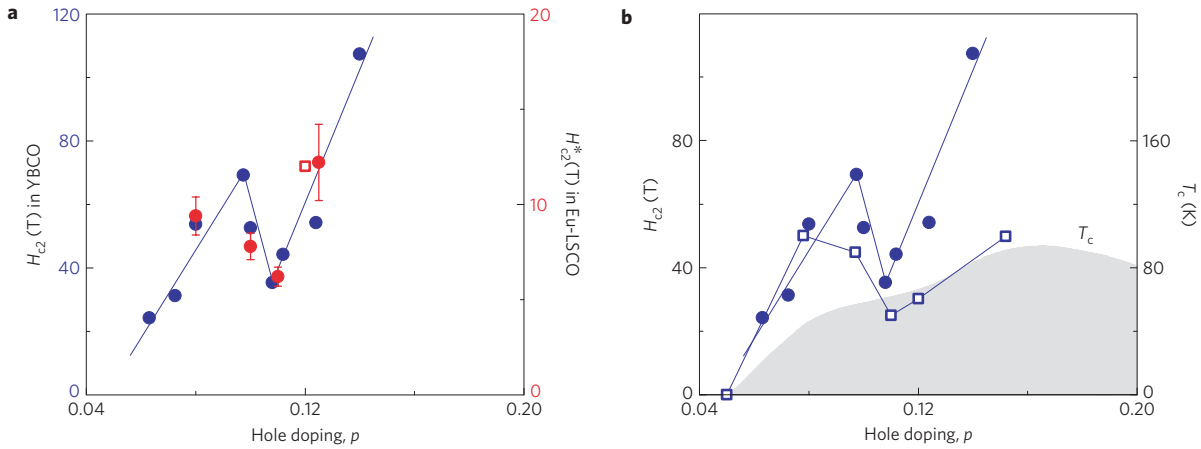

Figure 5 | Doping dependence of H_{c2} in YBCO and Eu-LSCO. a, Upper critical field H_{c2} obtained from the superconducting fluctuations above T_c, plotted as a function of hole doping p. For YBCO (blue symbols; left axis), H_{c2} is defined via the relation $H_{c2} \equiv \Phi_0/2\pi\xi_0^2$, in terms of the zero-temperature coherence length ξ_0 obtained from a Gaussian analysis of the fluctuation magneto-conductivity (ref. 7). For Eu-LSCO (red symbols; right axis), H_{c2} is taken to be H^*_{c2} in the fit of the peak field H^* to $H^* = H^*_{c2}\ln(T/T_c)$ (Fig. 3). Error bars on H^*_{c2} correspond to the uncertainty in fitting to the H^* data points in Fig. 3c. The red square marks the value of H_{c2} obtained directly from resistivity measurements at $T \to 0$ on Nd-LSCO, a material very similar to Eu-LSCO (Supplementary Fig. S6). **b**, Comparison of H_{c2} in YBCO determined in two different ways: from ξ_0 above T_c (circles), as in **a**, and from high-field transport measurements[23,24] (squares) that suppress superconductivity at low temperature ($T \ll T_c$). The two measures of H_{c2} are in reasonable agreement; in particular, they both have a minimum at $p = 0.11$, where $H_{c2} \approx 30$ T. The doping dependence of the zero-field T_c is shown for comparison (grey dome, right axis; ref. 34).

© 2012 Macmillan Publishers Limited. All rights reserved.

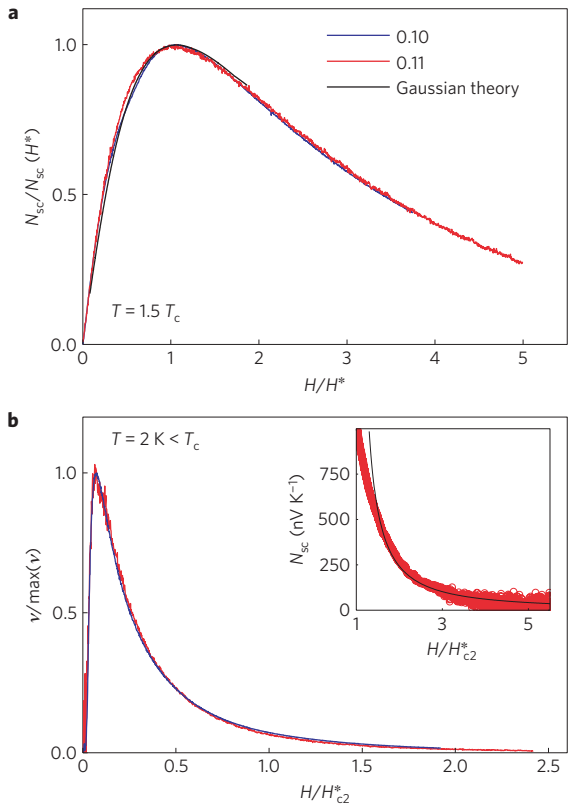

Figure 6 | Field dependence: comparison to Gaussian theory. a, Nernst signal N of Eu-LSCO at $p = 0.10$ (blue; $T_c = 5.0$ K) and $p = 0.11$ (red; $T_c = 3.86$ K) as a function of H/H^*, for a temperature $T = 1.5T_c$. At this temperature, the peak field H^*, at which N_{sc} versus H is maximal, is $H^* = 4.0$ T and 3.0 T, respectively. The solid line is a theoretical calculation of α_{xy}^{sc} ($=N_{sc}\sigma$), as in ref. 15, for a diffusion constant $D = 0.178$ cm^2 s^{-1} (K. Michaeli, personal communication). Note that the experimental σ at $T = 1.5T_c$ is essentially independent of H so that the H dependences of N_{sc} and α_{xy}^{sc} are the same. The theoretical curve is independent of D when normalized at H^*, for a wide range of D values (K. Michaeli, personal communication; Supplementary Fig. S7). **b**, Nernst coefficient of Eu-LSCO at $p = 0.10$ (blue) and $p = 0.11$ (red), for a temperature $T = 2\,\text{K} < T_c$, plotted versus H/H^*_{c2}, where H^*_{c2} is obtained from the peak field $H^* = H^*_{c2}\ln(T/T_c)$ (Fig. 3c). The fact that the data for different dopings collapse on the same curve when normalized by H^*_{c2} for both $T < T_c$ and $T > T_c$ (see also Supplementary Fig. S8) shows that H^*_{c2} is the relevant field scale throughout the H-T phase diagram. Inset: N_{sc} versus H/H^*_{c2} for $p = 0.11$ at the high-field end (up to 34 T), compared against the limiting behaviour expected theoretically[14,15] for $\alpha_{xy} = N_{sc}\sigma$ at $H \gg H_{c2}$, namely $\alpha_{xy} \sim 1/H\ln(H/H_{c2})$ (solid line).

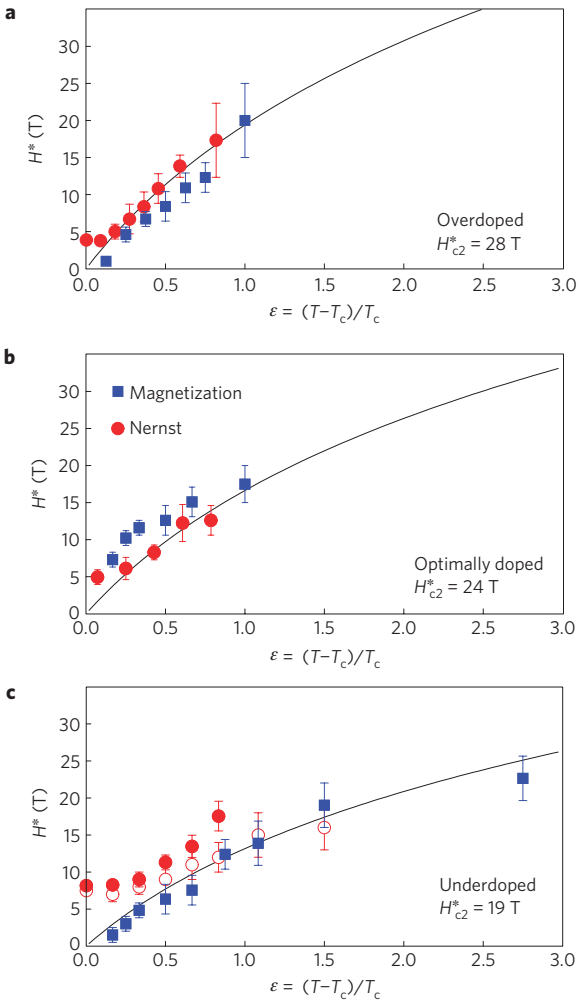

Figure 7 | Peak field H^* in Bi-2201. Peak field H^*, plotted versus $\varepsilon = (T - T_c)/T_c$, obtained from published data[10,20] on the cuprate Bi-2201, for three different dopings: **a**, overdoped ($T_c = 22$ K for Nernst[10] and $T_c = 20$ K for magnetization[20]), **b**, optimally doped ($T_c = 28$ K for Nernst[10] and $T_c = 30$ K for magnetization[20]), and **c** underdoped ($T_c = 12$ K for both Nernst[10] and magnetization[20]). H^* is extracted from Nernst data[10], as the peak in N versus H (filled red circles), and H^*_d is extracted from magnetization data[20], as the peak in the diamagnetic signal—$|M_d|$ versus H (blue squares). In the overdoped and optimally doped samples, where the quasiparticle term N_{qp} is very small[10], H^* agrees well with H^*_d (above $\varepsilon \approx 0.2$). In the underdoped sample ($T_c = 12$ K), however, a large positive N_{qp} must be subtracted to get a meaningful H^*, as in underdoped Eu-LSCO (Fig. 2). The open red circles are obtained assuming the same N_{qp} as in underdoped Eu-LSCO (Fig. 2a); they agree well with the magnetization data (blue squares). The solid lines are fits of the Nernst data to the expression $H^* = H^*_{c2}\ln(T/T_c)$, giving values of H^*_{c2} as indicated, with error bars of ±5 T. The fits reveal that H^*_{c2} decreases with decreasing p. The opposite conclusion would be reached if, as done previously[8], the focus were placed on the Nernst data at $T \approx T_c$ (Fig. 1b), where contamination by field-dependent paraconductivity is maximal (Supplementary Fig. S4). The error bars reflect the uncertainty in determining H^* from the data of refs 10 and 20.

$p \approx 0.11$, the vortex core radius is ≈3 nm, so that $H_{c2} \approx 30$ T (ref. 25). The fact that three very different measures of H_{c2} agree is compelling evidence that the correct value of H_{c2} has been reached in underdoped YBCO, with a minimum of $H_{c2} \approx 30$ T at $p = 0.11$. The agreement also confirms the validity of Gaussian theory. We conclude that the upper critical field H_{c2} of cuprates decreases with underdoping, in the same non-monotonic fashion in Eu–LSCO and YBCO.

We attribute this non-monotonic weakening of superconductivity to the competing effect of stripe order. Stripe order is present in Eu–LSCO above $p = 0.08$ (ref. 26). In YBCO, stripe order was recently inferred from Seebeck measurements of Fermi-surface reconstruction[24] and confirmed by high-field NMR measurements[27]. This scenario of phase competition is akin to that found in iron-based, heavy-fermion and organic superconductors, where the competing phase in these cases is spin-density-wave order. In YBCO at lower doping ($p < 0.08$), the rapid drop in T_c and H_{c2} (Fig. 5b) may be due to other phases, such as spin-density-wave order below $p \approx 0.08$ (ref. 28) and antiferromagnetism below $p \approx 0.05$. At low doping, the approach to the Mott insulator may also play a role.

© 2012 Macmillan Publishers Limited. All rights reserved.

Methods

Nernst effect. The Nernst effect[29] is the development of a transverse electric field E_y across the width (y axis) of a metallic sample when a temperature gradient $\partial T/\partial x$ is applied along its length (x axis) in the presence of a perpendicular magnetic field H (along the z axis). The Nernst signal is $N = E_y/(\partial T/\partial x)$ and the Nernst coefficient $\nu = N/H$. Two mechanisms can give rise to a Nernst signal: superconducting fluctuations, which give a positive signal N_{sc}, and charge carriers (quasiparticles), which give a signal N_{qp} that may be of either sign. The measured signal is their sum: $N = N_{sc} + N_{qp}$ (see Supplementary Information). The superconducting term N_{sc} is strongly dependent on the field strength H, whereas the quasiparticle term N_{qp} is essentially linear in field (that is, ν_{qp} is constant).

Samples. Single crystals of $La_{1.8-x}Eu_{0.2}Sr_xCuO_4$ (Eu–LSCO) were grown by the travelling floating zone method in Tokyo. The hole doping p is taken to be the nominal Sr concentration x. The characteristics of our four samples are listed in Supplementary Table S1. The superconducting transition temperature T_c was determined as the temperature below which the resistivity $\rho = 0$. For each sample, three pairs of silver epoxy contacts were diffused into the surface. Contacts used to measure the temperature gradient were separated by a distance L and the transverse contacts used to measure the Nernst voltage were separated by a distance w. The ratio L/w was typically in the range 0.5–3.

Single crystals of $La_{1.6-x}Nd_{0.4}Sr_xCuO_4$ (Nd–LSCO) used for determining H_{c2} from the resistivity (Supplementary Fig. S6) were described in ref. 30; their T_c and H_{c2} values are given in Supplementary Table S1.

Electrical resistivity. A standard four-probe method was used to measure the resistivity ρ in zero field. In Supplementary Fig. S3, we show ρ versus T for our four Eu–LSCO samples. Both temperature and doping dependences of the resistivity are consistent with published data[31], as is the magnitude just above T_c ($\rho \approx 1\,\mathrm{m}\Omega\,\mathrm{cm}$). The resistivity of Nd–LSCO samples is shown in Supplementary Fig. S6.

Nernst measurements. The Nernst effect was measured using a one-heater two-thermometer setup, as described in refs 32 and 33. The magnetic field, applied along the c axis, was swept between -15 and $+15$ T at a rate of $0.4\,\mathrm{T\,min^{-1}}$ or slower. Also, for Eu–LSCO samples with $p = 0.10$ and 0.125 ($p = 0.11$), the Nernst coefficient was measured up to 28 T (34 T) at the high-field laboratory in Grenoble Laboratoire National des Champs Magnétiques Intenses (LNCMI). Heat was applied horizontally in the ab plane and the temperature gradient $\mathrm{d}T = \Delta T/L$ was obtained by measuring the temperature difference ΔT between two contacts separated by the length L, using two uncalibrated Cernox chips referenced to a third calibrated chip. The Nernst voltage $V_y = E_y/w$ across two transverse contacts separated by the length w was measured using a nanovolt preamplifier and a nanovoltmeter.

The Nernst signal N is, as the Hall signal, anti-symmetric in field, so that by taking the difference

$$N = \{(V_y(H) - V_y(-H))/\mathrm{d}T\}(L/2w)$$

any symmetric component is eliminated. For example, contamination from the Seebeck effect due to slightly misaligned contacts is removed in this fashion. A constant background coming from the measurement circuit is also eliminated.

Received 12 April 2012; accepted 26 June 2012; published online 12 August 2012; corrected online 28 August 2012

References

1. Norman, M. R. *et al.* The pseudogap: Friend or foe of high T_c? *Adv. Phys.* **54,** 715–733 (2005).
2. Emery, V. J. & Kivelson, S. A. Importance of phase fluctuations in superconductors with small superfluid density. *Nature* **374,** 434–437 (1995).
3. Kanigel, A. *et al.* Evidence for pairing above the transition temperature of cuprate superconductors from the electronic dispersion in the pseudogap phase. *Phys. Rev. Lett.* **101,** 137002 (2008).
4. Chatterjee, U. *et al.* Observation of a d-wave nodal liquid in highly underdoped Bi2212. *Nature Phys.* **6,** 99–103 (2010).
5. Tanaka, K. *et al.* Distinct Fermi-momentum-dependent energy gaps in deeply underdoped Bi2212. *Science* **314,** 1910–1913 (2006).
6. Kondo, T. *et al.* Competition between the pseudogap and superconductivity in the high-T_c copper oxides. *Nature* **457,** 296–300 (2008).
7. Ando, Y. & Segawa, K. Magnetoresistance of untwinned $YBa_2Cu_3O_y$ single crystals in a wide range of doping: Anomalous hole-doping dependence of the coherence length. *Phys. Rev. Lett.* **88,** 167005 (2002).
8. Wang, Y. *et al.* Dependence of upper critical field and pairing strength on doping in cuprates. *Science* **299,** 86–89 (2003).
9. Xu, Z.A. *et al.* Vortex-like excitations and the onset of superconducting phase fluctuations in underdoped LSCO. *Nature* **406,** 486–488 (2000).
10. Wang, Y. *et al.* Nernst effect in high-T_c superconductors. *Phys. Rev. B* **73,** 024510 (2006).
11. Pourret, A. *et al.* Observation of the Nernst signal generated by fluctuating Cooper pairs. *Nature Phys.* **2,** 683–686 (2006).
12. Pourret, A. *et al.* Nernst effect as a probe of superconducting fluctuations in disordered thin films. *New J. Phys.* **11,** 055071 (2009).
13. Ussishkin, I., Sondhi, S. L. & Huse, D. A. Gaussian superconducting fluctuations, thermal transport, and the Nernst effect. *Phys. Rev. Lett.* **89,** 287001 (2002).
14. Serbyn, M. N. *et al.* Giant Nernst effect due to fluctuating Cooper pairs in superconductors. *Phys. Rev. Lett.* **102,** 067001 (2009).
15. Michaeli, K. & Finkel'stein, A. M. Fluctuations of the superconducting order parameter as an origin of the Nernst effect. *Europhys. Lett.* **86,** 27007 (2009).
16. Podolsky, D., Raghu, S. & Vishwanath, A. Nernst effect and diamagnetism in phase-fluctuating superconductors. *Phys. Rev. Lett.* **99,** 117004 (2007).
17. Pourret, A. *et al.* Length scale for the superconducting Nernst signal above T_c in $Nb_{0.15}Si_{0.85}$. *Phys. Rev. B* **76,** 214504 (2007).
18. Doiron-Leyraud, N. *et al.* Quantum oscillations and the Fermi surface in an underdoped high-T_c superconductor. *Nature* **447,** 565–568 (2007).
19. Sebastian, S. E. *et al.* Fermi-liquid theory in an underdoped high-T_c superconductor. *Phys. Rev. B* **81,** 140505 (2010).
20. Li, L. *et al.* Diamagnetism and Cooper pairing above T_c in cuprates. *Phys. Rev. B* **81,** 054510 (2010).
21. Wang, Y. *et al.* Field-enhanced diamagnetism in the pseudogap state of the cuprate superconductor $Bi_2Sr_2CaCu_2O_8$ in an intense magnetic field. *Phys. Rev. Lett.* **95,** 247002 (2005).
22. Schneider, T. & Weyeneth, S. Diamagnetism, Nernst signal, and finite-size effects in superconductors above the transition temperature T_c. *Phys. Rev. B* **83,** 144527 (2011).
23. LeBoeuf, D. *et al.* Lifshitz critical point in the cuprate superconductor $YBa_2Cu_3O_y$ from high-field Hall effect measurements. *Phys. Rev. B* **83,** 054056 (2011).
24. Laliberté, F. *et al.* Fermi-surface reconstruction by stripe order in cuprate superconductors. *Nature Commun.* **2,** 432 (2011).
25. Sonier, J. E. *et al.* Hole-doping dependence of the magnetic penetration depth and vortex core size in $YBa_2Cu_3O_y$: Evidence for stripe correlations near 1/8 hole doping. *Phys. Rev. B* **76,** 134518 (2007).
26. Fink, J. *et al.* Phase diagram of charge order in $La_{1.8-x}Eu_{0.2}Sr_xCuO_4$ from resonant soft x-ray diffraction. *Phys. Rev. B* **83,** 092503 (2011).
27. Wu, T. *et al.* Magnetic-field-induced charge-stripe order in the high-temperature superconductor $YBa_2Cu_3O_y$. *Nature* **477,** 191–194 (2011).
28. Haug, D. *et al.* Neutron scattering study of the magnetic phase diagram of underdoped $YBa_2Cu_3O_{6+x}$. *New J. Phys.* **12,** 105006 (2010).
29. Behnia, K. The Nernst effect and the boundaries of the Fermi-liquid picture. *J. Phys.: Condens. Matter* **21,** 113101 (2009).
30. Daou, R. *et al.* Linear temperature dependence of the resistivity and change in the Fermi surface at the pseudogap critical point of a high-T_c superconductor. *Nature Phys.* **5,** 31–34 (2009).
31. Hess, C. *et al.* Nernst effect of stripe ordering $La_{1.8-x}Eu_{0.2}Sr_xCuO_4$. *Eur. Phys. J. Spec. Top.* **188,** 103–112 (2010).
32. Cyr-Choinière, O. *et al.* Enhancement of the Nernst effect by stripe order in a high-T_c superconductor. *Nature* **458,** 743–745 (2009).
33. Daou, R. *et al.* Broken rotational symmetry in the pseudogap phase of a high-T_c superconductor. *Nature* **463,** 519–522 (2010).
34. Liang, R. *et al.* Evaluation of CuO_2 plane hole doping in $YBa_2Cu_3O_{6+x}$ single crystals. *Phys. Rev. B* **73,** 180505 (2006).

Acknowledgements

We thank H. Aubin, K. Behnia, A.M. Finkel'stein, V. Galitski, S. A. Kivelson, K. Michaeli, A. J. Millis, M. R. Norman, M. Serbyn, M. A. Skvortsov, A-M. Tremblay, D. van der Marel, A. Varlamov, and S. Weyerneth for fruitful discussions. We thank S. Y. Li for the resistivity data on Nd–LSCO (Supplementary Fig. S6) and J. Corbin for his assistance with the experiments. We thank K. Michaeli for her unpublished calculations in Fig. 6 and Supplementary Fig. S7. We thank the LNCMI for access to a high-field magnet allowing us to get data up to 28 T (Fig. 2) and 34 T (Fig. 6). J.C. was supported by Fellowships from the Fonds de recherche du Québec—Nature et technologies (FQRNT) and the Swiss National Foundation. E.H. was supported by a Fellowship from the FQRNT and a Junior Fellowship from the Canadian Institute for Advanced Research (CIFAR). L.T. acknowledges support from CIFAR and funding from the Natural Sciences and Engineering Research Council of Canada, FQRNT, the Canada Foundation for Innovation, and a Canada Research Chair.

Author contributions

J.C. initiated the project; J.C., N.D-L., O.C-C., F.L., E.H., J-Ph.R. and R.D. performed the Nernst measurements in Sherbrooke; J.C., N.D-L., F.L., O.C-C. and G.G. performed the Nernst measurements at the LNCMI in Grenoble; S.P., T.T. and H.T. prepared the Eu–LSCO samples and measured their resistivity; J.C., N.D-L. and L.T. analysed the data; J.C., N.D-L. and L.T. wrote the manuscript; L.T. supervised the project.

Additional information

Supplementary information is available in the online version of the paper. Reprints and permissions information is available online at www.nature.com/reprints. Correspondence and requests for materials should be addressed to L.T.

Competing financial interests

The authors declare no competing financial interests.

© 2012 Macmillan Publishers Limited. All rights reserved.

CORRIGENDUM

Decrease of upper critical field with underdoping in cuprate superconductors

J. Chang, N. Doiron-Leyraud, O. Cyr-Choinière, G. Grissonnanche, F. Laliberté, E. Hassinger, J-Ph. Reid, R. Daou, S. Pyon, T. Takayama, H. Takagi and Louis Taillefer

Nature Physics **8,** http://dx.doi.org/10.1038/nphys2380 (2012); published online 12 August 2012; corrected online 28 August 2012.

In the version of this Article originally published online, the unit on the *y* axis of Fig. 4c should have read ($m\Omega^{-1}$ cm^{-1}). This error has been corrected in the HTML and PDF versions of the Article.

© 2012 Macmillan Publishers Limited. All rights reserved.